Article

Magnetic Structure of the Large-Spin Mn and Mn Complexes: A Theoretical Complement to an Experimental Milestone

Eliseo Ruiz, Thomas Cauchy, Joan Cano, Ruben Costa, Javier Tercero, and Santiago Alvarez

J. Am. Chem. Soc., **2008**, 130 (23), 7420-7426 • DOI: 10.1021/ja800092s • Publication Date (Web): 20 May 2008

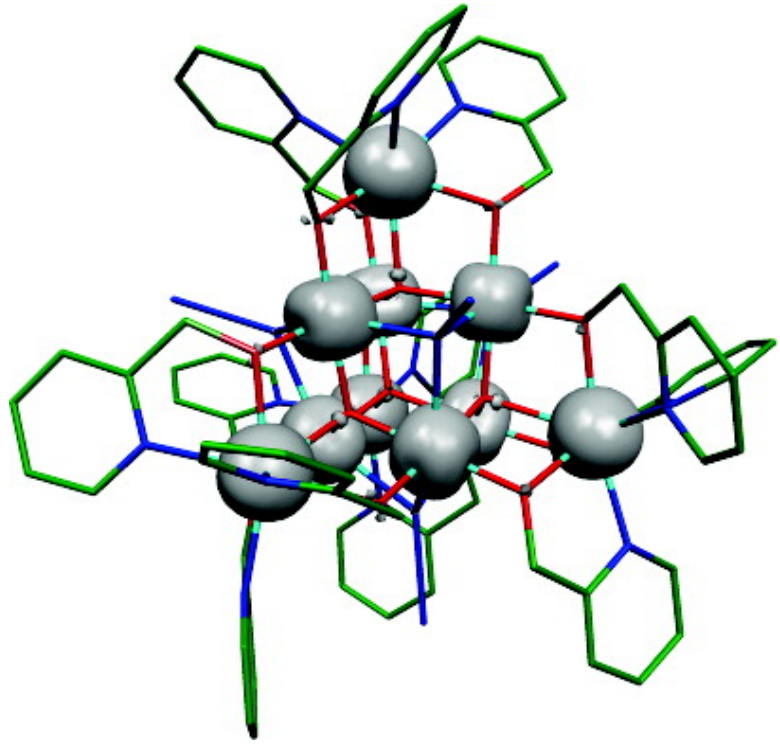

J|A|C|S
ARTICLES

Published on Web 05/20/2008

Magnetic Structure of the Large-Spin Mn_{10} and Mn_{19} Complexes: A Theoretical Complement to an Experimental Milestone

Eliseo Ruiz,*,† Thomas Cauchy,† Joan Cano,‡ Ruben Costa,† Javier Tercero,† and Santiago Alvarez†

Departament de Química Inorgànica and Institut de Recerca de Química Teòrica i Computacional, Universitat de Barcelona, Diagonal 647, 08028 Barcelona, Spain, and Institució Catalana de Recerca i Estudis Avançats (ICREA), Passeig Lluís Companys 23, 08010 Barcelona, Spain

Received January 5, 2008; E-mail: eliseo.ruiz@qi.ub.es

Abstract: High-spin molecules have been proposed as candidates for the storage of information at the molecular level. The electronic structure of two complex magnetic molecular systems, Mn_{10} and Mn_{19}, is characterized by means of a computational study based on density functional theory. All the exchange interactions in the recently reported Mn_{19} complex with the highest known spin value of 83/2, and in its highly symmetric Mn_{10} parent compound, are ferromagnetic. In these complexes, there are two kinds of ferromagnetic coupling: the first one corresponds to $Mn^{II}-Mn^{III}$ interactions through a double μ_2-alkoxo-μ_4-oxo bridge where the high coordination number of the Mn^{II} cations results in long $Mn^{II}-O$ bond distances, while the second one involves $Mn^{III}-Mn^{III}$ interactions through μ_2-alkoxo-μ_3-η^1:η^1:η^1 azido bridging ligands with long $Mn^{III}-N$ distances due to a Jahn−Teller effect.

Introduction

Two related mixed-valence $Mn^{II}-Mn^{III}$ polynuclear complexes, Mn_{10} and Mn_{19},[1,2] with large values of the total spin in their ground states, have been recently reported. The latter is so far the world record for molecular spin, with $S = 83/2$, significantly surpassing the previous highest values of $S = 51/2$ and $S = 61/2$ in Mn_{25} complexes.[3,4] Such high-spin polynuclear transition metal complexes are much sought after synthetic targets, due to their potential as single-molecule magnets (SMM) that could eventually lead to applications for information storage at the molecular level. Slow relaxation of the magnetization of such compounds at low temperature is responsible for the presence of a hysteresis loop in their magnetization curves, a characteristic behavior of magnets that used to be associated with bulk materials only. In order to have a slow relaxation of the magnetization, the states with positive and negative magnetic moments must be separated by an energy barrier, the height of which is known to depend directly on the square of the total spin of the molecule and its magnetic anisotropy.[5,6] Hence the importance of having molecules with such large spins as Mn_{19}, even if in this case the magnetic anisotropy is so small that no SMM behavior is clearly observed.

In the efforts toward preparing polynuclear complexes with high spin, a common shortcoming is that the local spins of the metal atoms are antiferromagnetically coupled and the total spin in the ground state is not as large as it could be if the coupling was ferromagnetic. As an example, in the paradigmatic $[Mn_{12}O_{12}(CH_3COO)_{16}(H_2O)_4]$ complex known as Mn_{12},[7] the ground state has $S = 10$, rather than its highest spin state $S = 22$. In contrast, the most salient feature of Mn_{19} and Mn_{10} is that their magnetic behavior is compatible only with the highest possible spin, indicating that all the Mn atoms therein are ferromagnetically coupled. Therefore, a full characterization of the exchange interactions that determine such high spin states, not directly obtainable from the temperature dependence of the magnetic susceptibility, should provide us with valuable information for the future design of new molecular systems with still higher spin.

The goals of the present work are to study the magnetic properties of the Mn_{19} and Mn_{10} complexes using theoretical methods based on density functional theory (DFT), to establish the sign and magnitude of the exchange coupling constants (J) within such systems, and to search for the structural factors that determine their ferromagnetic nature. To that end, we apply the computational tools that have successfully described the electronic and magnetic structures

† Universitat de Barcelona.
‡ ICREA.

(1) Ako, A. M.; Hewitt, I. J.; Mereacre, V.; Clérac, R.; Wensdorfer, W.; Anson, C. E.; Powell, A. K. *Angew. Chem., Int. Ed.* **2006**, *45*, 4926–4929.
(2) Stamatatos, T. C.; Abboud, K. A.; Wensdorfer, W.; Christou, G. *Angew. Chem., Int. Ed.* **2006**, *45*, 4134–4137.
(3) Murugesu, M.; Habrych, M.; Wernsdorfer, W.; Abboud, K. A.; Christou, G. *J. Am. Chem. Soc.* **2004**, *126*, 4766–4767.
(4) Stamatatos, T. C.; Abboud, K. A.; Wensdorfer, W.; Christou, G. *Angew. Chem., Int. Ed.* **2006**, *46*, 884–888.
(5) Sessoli, R.; Gatteschi, D. *Angew. Chem., Int. Ed.* **2003**, *42*, 268–297.
(6) *Magnetism: Molecules to Materials*; Miller, J. S., Drillon, M., Eds.; Wiley-VCH: Weinheim, 2001−2005; Vols. 1−5.
(7) Caneschi, A.; Gatteschi, D.; Sessoli, R.; Barra, A. L.; Brunel, L. C.; Guillot, M. *J. Am. Chem. Soc.* **1991**, *113*, 5873–5874.

 10.1021/ja800092s CCC: $40.75

of a variety of polynuclear transition metal complexes.[8–11] In particular, we have found that codes that use numerical or plane waves basis sets with generalized gradient approximation (GGA) exchange-correlation functionals, such as that proposed by Perdew−Burke−Ernzerhof (PBE),[12] provide very good results for large molecules,[13,14] while the hybrid B3LYP functional together with Gaussian basis sets have become the standard method for not-so-large systems. Here, we report on calculations with numerical basis sets and the PBE functional as well as computations with a Gaussian basis set and the B3LYP method for the Mn_{10} and Mn_{19} complexes. Details of such calculations and results for dinuclear compounds showing the excellent agreement with experimental data reached with the PBE functional and numerical basis sets are included in the Computational Details section.

Results and Discussion

Analysis of the Topology of the Complexes. The molecular structures of the Mn_{19} and Mn_{10} complexes are represented in Figure 1. Both have as a common motif a Mn_{10} core that can be described as a supertetrahedron with Mn^{II} cations at the vertices and Mn^{III} cations at the edges, the latter having perforce an octahedral arrangement.[15] The Mn_{19} complex can be simply described as the result of the condensation of two such Mn_{10} cores, sharing one of the Mn^{II} vertices. The shared Mn^{II} cation presents an uncommon cubic coordination sphere, while the other Mn^{II} cations are seven-coordinated with a capped octahedral coordination, and the Mn^{III} ions present distorted octahedral coordination spheres. The two complexes have very similar bridges, including μ_3-η^1:η^1:η^1 azido ligands coordinated to the Mn^{III} cations, i.e., capping the faces of the $Mn^{III}{}_6$ octahedra not occupied by Mn^{II} ions. It is precisely the presence of such bridging azido ligands that has been blamed for the ferromagnetism found, since these ligands have a well-known tendency to favor ferromagnetic coupling in dinuclear complexes.[16]

The spin Hamiltonian for a general polynuclear complex can be expressed as

$$\hat{H} = -\sum_{i>j} J_{ij}\hat{S}_i\hat{S}_j + D\left(\hat{S}_z^{\,2} - \frac{1}{2}\hat{S}^2\right) + E\left(\hat{S}_x^{\,2} - \hat{S}_y^{\,2}\right) \qquad (1)$$

where $\hat{S}_i$ and $\hat{S}_j$ are the spin operators of the paramagnetic centers i and j and $\hat{S}$ and $\hat{S}_z$ are the total spin operator of the molecule and its axial component, respectively. The J_{ij} values are the exchange coupling constants for the different pairwise interactions between the paramagnetic centers of the molecule, while D and E are the axial and rhombic components of the anisotropy, respectively. The spin−orbit coupling effects must be taken into account for the calculation of the zero-field-splitting (ZFS) D and E parameters.[17,18] Such effects are not included in our calculation; hence, by neglecting ZFS, we can obtain directly the energy values to calculate the exchange coupling. Although our main objective is the Mn_{19} complex, from here on we will proceed in order of increasing complexity, analyzing first our results for Mn_{10}. According to the description of the structure above, only two different exchange interactions appear in Mn_{10}, thanks to its high symmetry (Figure 2a), and the spin Hamiltonian, considering only the exchange coupling terms, can be expressed by eq 2:

$$\begin{aligned}\hat{H} = -J_a[&\hat{S}_5\hat{S}_6 + \hat{S}_5\hat{S}_7 + \hat{S}_5\hat{S}_8 + \hat{S}_5\hat{S}_{10} + \hat{S}_6\hat{S}_7 + \hat{S}_6\hat{S}_8 + \\ &\hat{S}_6\hat{S}_9 + \hat{S}_7\hat{S}_9 + \hat{S}_7\hat{S}_{10} + \hat{S}_8\hat{S}_9 + \hat{S}_8\hat{S}_{10} + \hat{S}_9\hat{S}_{10}] - \\ J_b[&\hat{S}_1\hat{S}_5 + \hat{S}_1\hat{S}_6 + \hat{S}_1\hat{S}_7 + \hat{S}_2\hat{S}_5 + \hat{S}_2\hat{S}_8 + \hat{S}_2\hat{S}_{10} + \\ &\hat{S}_3\hat{S}_6 + \hat{S}_3\hat{S}_8 + \hat{S}_3\hat{S}_9 + \hat{S}_4\hat{S}_7 + \hat{S}_4\hat{S}_9 + \hat{S}_4\hat{S}_{10}] \end{aligned} \qquad (2)$$

where $\hat{S}_i$ are the local spin operators of each paramagnetic center. The first term corresponds to Mn^{III}−Mn^{III} and the second one to Mn^{III}−Mn^{II} interactions. In the case of the Mn_{19} complex, we have essentially the same two types of interactions, but four different exchange coupling constants must be considered for each because of the lower symmetry: J_1−J_4 for the Mn^{III}−Mn^{III} and J_5−J_8 for the Mn^{III}−Mn^{II} interactions, as schematically

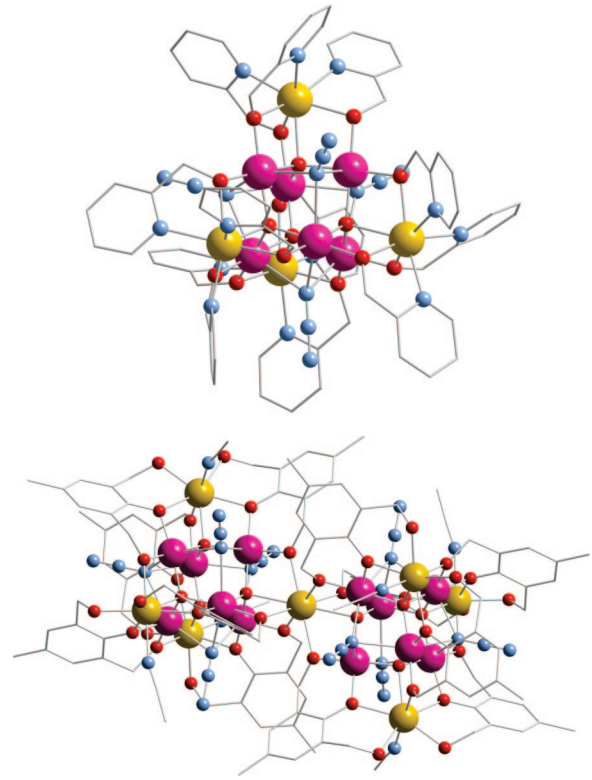

Figure 1. Molecular structures of the Mn_{19} complex, $[Mn^{II}{}_7Mn^{III}{}_{12}(\mu_4\text{-}O)_8(\mu_3\text{-}N_3)_8(HL)_{12}(MeCN)_6]^{2+}$ (H_3L = 2,6-bis(hydroxymethyl)-4-methylphenol) (below), and of its parent Mn_{10} compound, $[Mn^{II}{}_4Mn^{III}{}_6(\mu_4\text{-}O)_4(\mu_3\text{-}N_3)_4(hmp)_{12}]^{2+}$ (hmp = 2-(hydroxymethyl)pyridine) (above). The Mn^{II} and Mn^{III} cations, oxygen atoms, and nitrogen atoms are represented as yellow, pink, red, and blue spheres, respectively, while hydrogen atoms are omitted for clarity.

(8) Postnikov, A. V.; Kortus, J.; Pederson, M. R. *Phys. Stat. Sol. B* **2006**, *243*, 2533–2572.
(9) Ruiz, E.; Alvarez, S.; Rodríguez-Fortea, A.; Alemany, P.; Pouillon, Y.; Massobrio, C. In *Magnetism: Molecules to Materials*; Miller, J. S., Drillon, M., Eds.; Wiley-VCH: Weinheim, 2001; Vol. 2, p 227.
(10) Ruiz, E.; Alemany, P.; Alvarez, S.; Cano, J. *J. Am. Chem. Soc.* **1997**, *119*, 1297–1303.
(11) Ruiz, E. *Struct. Bonding (Berlin)* **2004**, *113*, 71–102.
(12) Perdew, J.; Burke, K.; Ernzerhof, M. *Phys. Rev. Lett.* **1996**, *77*, 3865–3868.
(13) Massobrio, C.; Ruiz, E. *Monatsh. Chem.* **2003**, *134*, 317–326.
(14) Ruiz, E.; Rodríguez-Fortea, A.; Tercero, J.; Cauchy, T.; Massobrio, C. *J. Chem. Phys.* **2005**, *123*, 074102.
(15) Alvarez, S. *Dalton Trans.* **2005**, 2209–2233.
(16) Ruiz, E.; Cano, J.; Alvarez, S.; Alemany, P. *J. Am. Chem. Soc.* **1998**, *120*, 11122.
(17) Pederson, M. R.; Khanna, S. N. *Phys. Rev. B* **1999**, *60*, 9566–9572.
(18) Kortus, J.; Pederson, M. R.; Baruah, T.; Bernstein, N.; Hellberg, C. S. *Polyhedron* **2003**, *22*, 1871–1876.

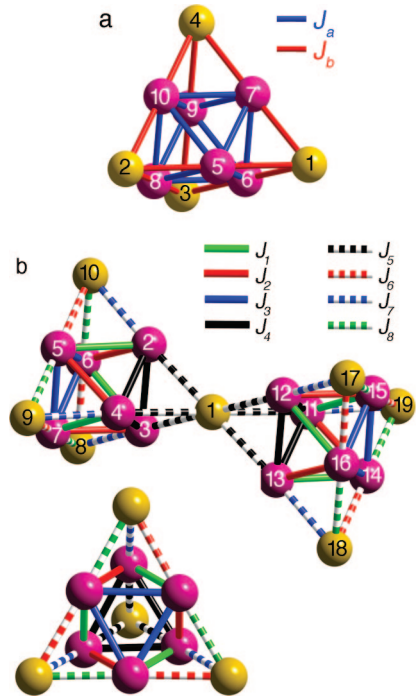

Figure 2. Schemes showing the topology of the exchange interactions in the two studied complexes: (a) Mn_{10} and (b) Mn_{19}. Yellow spheres, Mn^{II}; pink spheres, Mn^{III}.

represented in Figure 2b, with the corresponding spin Hamiltonian:

$$\begin{aligned}\hat{H} = &-J_1[\hat{S}_2\hat{S}_5 + \hat{S}_3\hat{S}_6 + \hat{S}_4\hat{S}_7 + \hat{S}_{11}\hat{S}_{15} + \hat{S}_{12}\hat{S}_{16} + \hat{S}_{13}\hat{S}_{14}] - \\ &J_2[\hat{S}_2\hat{S}_6 + \hat{S}_3\hat{S}_7 + \hat{S}_4\hat{S}_5 + \hat{S}_{11}\hat{S}_{14} + \hat{S}_{12}\hat{S}_{15} + \hat{S}_{13}\hat{S}_{16}] - \\ &J_3[\hat{S}_2\hat{S}_3 + \hat{S}_2\hat{S}_4 + \hat{S}_3\hat{S}_4 + \hat{S}_{11}\hat{S}_{12} + \hat{S}_{11}\hat{S}_{13} + \hat{S}_{12}\hat{S}_{13}] - \\ &J_4[\hat{S}_5\hat{S}_6 + \hat{S}_5\hat{S}_7 + \hat{S}_6\hat{S}_7 + \hat{S}_{14}\hat{S}_{15} + \hat{S}_{14}\hat{S}_{16} + \hat{S}_{15}\hat{S}_{16}] - \\ &J_5[\hat{S}_1\hat{S}_2 + \hat{S}_1\hat{S}_3 + \hat{S}_1\hat{S}_4 + \hat{S}_1\hat{S}_{11} + \hat{S}_1\hat{S}_{12} + \hat{S}_1\hat{S}_{13}] - \\ &J_6[\hat{S}_5\hat{S}_{10} + \hat{S}_6\hat{S}_8 + \hat{S}_7\hat{S}_9 + \hat{S}_{14}\hat{S}_{18} + \hat{S}_{15}\hat{S}_{19} + \hat{S}_{16}\hat{S}_{17}] - \\ &J_7[\hat{S}_2\hat{S}_{10} + \hat{S}_3\hat{S}_8 + \hat{S}_4\hat{S}_9 + \hat{S}_{11}\hat{S}_{19} + \hat{S}_{12}\hat{S}_{17} + \hat{S}_{13}\hat{S}_{18}] - \\ &J_8[\hat{S}_5\hat{S}_9 + \hat{S}_6\hat{S}_{10} + \hat{S}_7\hat{S}_8 + \hat{S}_{14}\hat{S}_{19} + \hat{S}_{15}\hat{S}_{17} + \hat{S}_{16}\hat{S}_{18}] \qquad (3)\end{aligned}$$

Exchange Interactions in the Mn_{10} Complex. The exchange coupling constants of the Mn_{10} complex have been calculated considering the $[Mn^{II}_4Mn^{III}_6(\mu_4\text{-}O)_4(\mu_3\text{-}N_3)_4(hmp)_{12}]^{2+}$ cation in full, neglecting the perchlorate counterions, which have been seen to have a negligible influence on the exchange coupling (see below). From the calculated J values (Table 1), we can conclude that the two DFT approaches employed give similar results and that the two interactions are ferromagnetic, resulting in an $S = 22$ ground state, as experimentally found. The fact that J_a is larger than J_b may be associated with the presence of end-on azido bridges in the J_a exchange pathway. Indeed, despite the long Mn−N bond distances (2.416 Å), we find that such bridging ligands play an important role, since in their absence we calculate a negative value for J_a (Table 2). However, replacement of the bridging azides by other end-on ligands, such as OH^- or SCN^-, results in similar ferromagnetic interactions (Table 2). This fact has been recently confirmed by a new Mn_{10} complex, with a similar structure but with disordered bromide and hydroxo bridging ligands, that also presents ferromagnetic interactions and an $S = 22$ ground state.[19]

Table 1. Exchange Coupling Constants (J, cm^{-1}) for the Two Exchange Pathways in the Mn_{10} Ion, $[Mn^{II}_4Mn^{III}_6(\mu_4\text{-}O)_4(\mu_3\text{-}N_3)_4(hmp)_{12}]^{2+}$, and Atomic Spin Populations (ρ) Calculated with the PBE Functional and the Siesta Code and with the B3LYP Functional and the Gaussian Program; The Set of Bridging Ligands Associated with Each Coupling Constant and the Corresponding Geometrical Parameters Are Also Given (Distances in Angstroms, Bond Angles in Degrees)

	bridging ligands	Mn···Mn	Mn—X[b]	Mn—X—Mn	PBE	B3LYP
J_a	μ_4-O, μ_3-N_3	3.239	1.907, 2.416	116.3, 84.2	23.2	15.9
J_b	μ_4-O, μ-OR	3.267	1.907, 1.889	101.2, 104.5	3.7	1.6
			2.308, *2.233*			
$\rho(Mn^{II})$					4.67	4.88
$\rho(Mn^{III})$					3.84	3.94

[a] See Computational Details. [b] Values in italics correspond to the Mn^{II} cations.

Table 2. Calculated Exchange Coupling Constants J (cm^{-1}) and Metal Spin Populations for the Whole Mn_{10} Complex, $[Mn^{II}_4Mn^{III}_6O_4(N_3)_4(hmp)_{12}]^{2+}$, Using Numerical Basis Sets (Siesta Code)[a]

	full molecule	$+2ClO_4^-$	$-4N_3^-$	$+4OH^-$	$+4NCS^-$
J_a	23.2	23.6	−7.7	19.0	20.3
J_b	3.7	3.3	9.0	3.7	4.1
ρ (Mn^{II})	4.67	4.66	4.58	4.66	4.66
ρ (Mn^{III})	3.84	3.84	4.03	3.88	3.83

[a] Additional systems were calculated to check the influence of added perchlorate counteranions: a system without the azido bridging ligands and two cases with OH^- and SCN^- bridging ligands replacing the azido groups to check their influence on the exchange coupling constants.

The weak ferromagnetic interaction revealed by the small positive J_b value is interesting, since Mn^{II} cations usually present antiferromagnetic coupling. This result might be associated with the interaction with a Mn^{III} cation with a small antiferromagnetic contribution due to the presence of only one unpaired electron at the "e_g" orbitals, as well as to the long Mn^{II}—O bond distances (Table 1) caused by the high coordination number of the Mn^{II} cations. Dinuclear mixed-valence alkoxo-bridged Mn^{II}—Mn^{III} complexes have been reported[20,21] that show weak ferromagnetic coupling, consistent with our theoretical results and the experimental data for the J_b interaction in the Mn_{10} complex.

Finally, the analysis of the spin population distribution indicates a strong localization of the spin density at the metal atoms, especially in the case the Mn^{III} cations, that can be explained by their $t_{2g}^3\ e_g^1$ electron configuration, in which three unpaired electrons occupy the nonbonding t_{2g} orbitals and one is in the antibonding M—L d_{z^2} orbital that is weakly delocalized due to the long Mn—N bond distances.[22,23] Such a large spin localization is likely to favor a ferromagnetic coupling, as seen earlier for other Mn^{II} complexes with high coordination num-

(19) Manoli, M.; Johnstone, R. D. L.; Parsons, S.; Murrie, M.; Affronte, M.; Evangelisti, M.; Brechin, E. K. *Angew. Chem., Int. Ed.* **2007**, *46*, 4456–4460.
(20) Bashkin, J. S.; Schake, A. R.; Vincent, J. B.; Chang, H.-R.; Li, Q.; Huffman, J. C.; Christou, G.; Hendrickson, D. N. *Chem. Commun.* **1988**, 700–702.
(21) Gelasco, A.; Kirk, M. L.; W, K. J.; Pecoraro, V. L *Inorg. Chem.* **1997**, *36*, 1829–1837.
(22) Cano, J.; Ruiz, E.; Alvarez, S.; Verdaguer, M. *Comments Inorg. Chem.* **1998**, *20*, 27–56.
(23) Ruiz, E.; Cirera, J.; Alvarez, S. *Coord. Chem. Rev.* **2005**, *249*, 2649–2660.

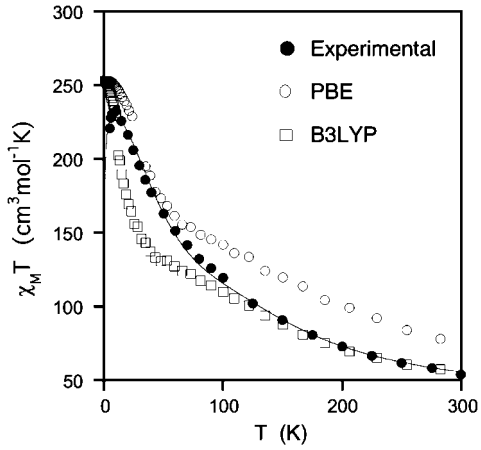

Figure 3. Temperature dependence of the magnetic susceptibility of the Mn_{10} complex, from experiment (●; solid line for the least-squares fitting) and from a combined quantum Monte Carlo simulation and exact diagonalization approach (see text for details) using the coupling constants calculated with the PBE (○) and B3LYP (□) functionals and the associated methodologies described in the text.

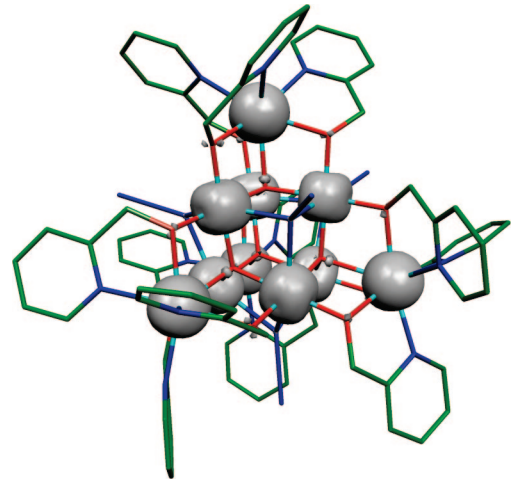

Figure 4. Spin density map for the $S = 22$ ground state of the Mn_{10} complex, calculated with the B3LYP functional. The isodensity surface represented corresponds to a value of 0.03 e^-/bohr^3 (gray regions indicate positive spin populations; negative values are not detected with the cutoff employed).

ber.[24] To check this conclusion, we recalculated the J values using a model structure in which the Mn−O bond distances were reduced to 2.08 Å, in which case an antiferromagnetic coupling constant was obtained, thus confirming the importance of the long Mn−O bond distances associated with the high coordination number of the Mn^{II} cations.

In order to verify the accuracy of the calculated J values, we wish to compare the experimental magnetic susceptibility curve with that obtained from calculated coupling constants. The neglected ZFS terms are very small for these high-spin molecules; consequently, their influence on the magnetic susceptibility curve is negligible. Since the large size of the Hamiltonian matrix prevents the exact diagonalization of the whole matrix, we have combined quantum Monte Carlo simulations that properly describe the magnetic susceptibility curve at high temperatures with the exact diagonalization corresponding to the lowest energy states (from $S = 22$ to $S = 12$, with relatively small matrices) that is expected to correctly simulate the low-temperature region (below 20 K). Among the possible quantum Monte Carlo methods, we have used the decoupled cell method (DCM) as proposed by Homma et al.[25,26] In this method, the probability of inverting the M_S values (spin flip) for a site is evaluated from the probabilities obtained in a subsystem in which this site occupies the central position. These probabilities are also evaluated by the exact diagonalization applied to that specific subsystem. The Monte Carlo simulations were carried out in a way similar to that described in previous work, using in this case 5×10^5 steps.[27]

The experimental curve (Figure 3) is bound by the two sets of calculated data, with the high-temperature zone being best reproduced by the B3LYP method and the low-temperature zone by the PBE approach. The different behavior of the two sets of calculated J values suggests that the larger coupling constant J_a, which dominates the shape of the curve at high temperatures, is best reproduced by the B3LYP calculations, whereas for the smaller J_b, which should become more relevant at low temperatures, the PBE approach seems to give a better agreement. This combined approach of quantum Monte Carlo simulations and exact diagonalization has been employed to perform a fitting of the experimental data, obtaining $J_a = 16.7$ cm^{-1}, $J_b = 2.5$ cm^{-1}, $g = 1.943$, and an intermolecular interaction term $\theta = -0.20$ cm^{-1} ($R = 2.8 \times 10^{-4}$). These values confirm the conclusion that the B3LYP J_a value agrees better with the experimental data at high temperature, while the three J_b values are rather similar. Those results also show how sensitive the magnetic behavior is to differences of a few wavenumbers in the coupling constants. Using the eigenvalues corresponding to the exact diagonalization of the smallest blocks, the excitation energy between the $S = 22$ ground state and the $S = 21$ first excited state are 18.4 and 5.4 cm^{-1} with the PBE and B3LYP J values, respectively.

The representation of the spin density calculated for the Mn_{10} complex in its $S = 22$ ground state (Figure 4) reveals a strong localization of the unpaired electrons at the manganese cations. Thus, the peripheral Mn^{II} cations have an almost perfect spherical spin distribution, while at the central Mn^{III} ones it is slightly distorted due to the d^4 electron configuration.[22,23] The spin delocalization over the ligands is very small due to the long Mn^{III}−N and Mn^{II}−O bond distances that result in a poor mixing between the ligand and manganese 3d orbitals in the antibonding molecular orbitals responsible for the spin delocalization. It is possible to detect tiny positive spin densities at the oxo bridging ligand, while practically no spin density is seen at the azido bridges. In summary, the long Mn−X bond distances in Mn_{10} result in an important metal-centered localization of the unpaired electrons, thus accounting for small antiferromagnetic contributions, and ferromagnetic interactions predominate.

Exchange Interactions in the Mn_{19} Complex. Now that we have seen how well the low-temperature magnetic behavior is reproduced by the DFT methodology for Mn_{10}, we can look at the results for the more complex Mn_{19} molecule. The calculated J values (Table 3) follow trends similar to those found above for Mn_{10}: (i) all the exchange coupling constants are ferromag-

(24) Gillon, B.; Mathoniere, C.; Ruiz, E.; Alvarez, S.; Cousson, A.; Rajendiran, T. M.; Kahn, O. *J. Am. Chem. Soc.* **2002**, *124*, 14433–14441.
(25) Homma, S. In *Quantum Monte Carlo Methods in Condensed Matter Physics*; Suzuki, M., Ed.; World Scientific Publishing Co. Pte. Ltd.: Singapore, 1993.
(26) Homma, S.; Matsuda, H.; Ogita, N. *Prog. Theor. Phys.* **1986**, *75*, 1058–1065.
(27) Ruiz, E.; Cano, J.; Alvarez, S. *Chem. Eur. J.* **2005**, *11*, 4767.

Table 3. Calculated Exchange Coupling Constants J (cm^{-1}) for the Mn_{19} Complex Mediated by Different Pairs of Bridging Ligands, Together with the Corresponding Geometrical Parameters[a]

	bridging ligands	Mn···Mn (Å)	Mn−X[b] (Å)	Mn−X−Mn (°)	J_{PBE}	J_{B3LYP}
			Mn^{III}−Mn^{III}			
J_1	μ_4-O, μ_3-N_3	3.311	1.929, 1.923, 2.473, 2.456	118.5, 84.4	9.9	3.0
J_2	μ_4-O, μ_3-N_3	3.219	1.929, 1.905, 2.500, 2.456	114.3, 81.0	15.7	15.2
J_3	μ_4-O, μ_3-N_3	3.206	1.891, 1.891, 2.500, 2.473	115.9, 80.3	16.8	11.3
J_4	μ_4-O, μ_3-N_3	3.185	1.923, 1.904, 2.363, 2.363	112.7, 84.7	22.2	14.0
			Mn^{II}−Mn^{III}			
J_5	μ_4-O, μ-OR	3.436	1.891, 1.854, *2.509*, *2.345*	101.8, 109.3	3.6	1.8
J_6	μ_4-O, μ-OR	3.303	1.923, 1.895, *2.262*, *2.362*	104.0, 101.3	7.2	5.4
J_7	μ_4-O, μ-OR	3.298	1.929, 1.894, *2.262*, *2.286*	103.5, 103.8	7.2	3.4
J_8	μ_4-O, μ-OR	3.224	1.904, 1.878, *2.262*, *2.186*	101.1, 104.8	5.1	1.6

[a] The coupling constants were obtained using the PBE functional and the Siesta code and with the B3LYP functional and the NWChem code (see Computational Details). [b] Values in italics correspond to the Mn^{II} cations.

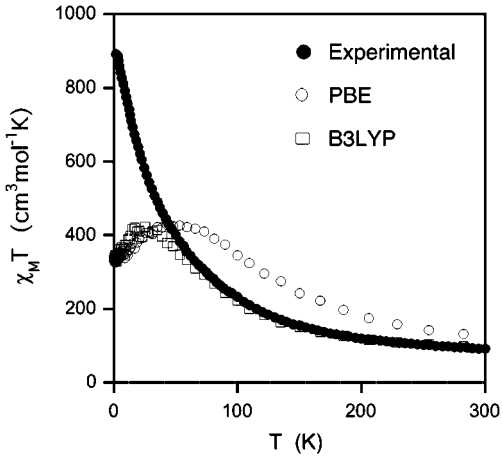

Figure 5. Temperature dependence of the magnetic susceptibility of the Mn_{19} complex, from experiment (●) and from quantum Monte Carlo simulations using the coupling constants calculated with the PBE (○) and B3LYP (□) functionals and the associated methodologies described in the text.

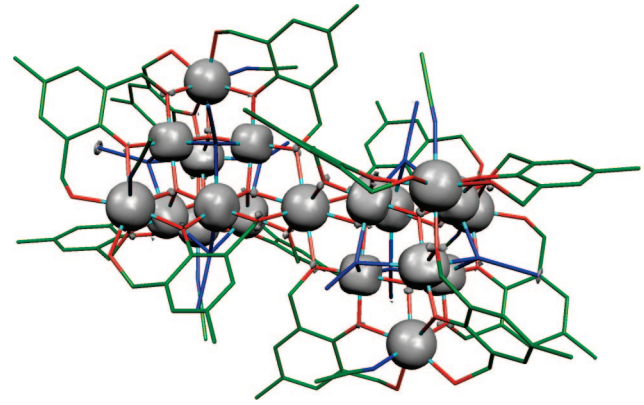

Figure 6. Spin density map for the $S = 83/2$ ground state of the Mn_{19} complex, calculated with the B3LYP functional. The isodensity surface represented corresponds to a value of 0.03 $e^-/bohr^3$ (gray regions indicate positive spin populations; negative values are not detected with the employed cutoff).

netic, in agreement with the $S = 83/2$ ground state that is consistent with the experimental data;[1] (ii) the J_1-J_4 interactions between pairs of octahedral Mn^{III} ions through μ_4-O and μ_3-N_3 bridges (equivalent to J_a in Mn_{10}) are the strongest ones, even if there are significant differences in their numerical values that could be associated with differences in the Mn···Mn distances, at least in the PBE results; (iii) the interactions through μ_4-O and μ-OR bridges between the external seven-coordinated Mn^{II} ions and the octahedral Mn^{III} ions (J_6-J_8, analogous to J_b in Mn_{10}) are weaker (6 ± 1 cm^{-1}); and (iv) the J_5 interaction involving the central octacoordinated Mn^{II} cation shows a weaker ferromagnetic coupling than those corresponding to the heptacoordinated Mn^{II} cations (J_6-J_7). Although the ferromagnetic nature of the J_5-J_8 coupling constants may seem somewhat odd, given the antiferromagnetic interactions usually found through μ_4-O and μ-OR bridges, such a difference could be attributed to the presence of a long Mn^{II}−X distance to each bridging ligand, as discussed in the previous section.

In order to compare our theoretical results with the magnetic susceptibility curve, we performed quantum Monte Carlo simulations with the two sets of calculated J values, and the results are represented in Figure 5. In this case, the number of states is too large, and it is not possible to perform a significant number of block diagonalizations of the highest spin states to describe the low-temperature regime, as done above for the Mn_{10} complex. It is well known that quantum Monte Carlo simulations fail at low temperatures;[27] however, the agreement between the experimental curve and that obtained with the B3LYP J values is excellent down to 40 K. The curve obtained with the PBE functional corroborates also the results of Mn_{10} complex at high temperature, showing that the J_1-J_4 values are too ferromagnetic.

The representation of the spin density calculated for the Mn_{19} complex in its $S = 83/2$ ground state (Figure 6) indicates a strong localization of the unpaired electrons at the manganese cations, as in the Mn_{10} complex. Small delocalization contributions appear at the oxo bridging ligands and at the third nitrogen atom of the μ_3-η^1:η^1:η^1 azido bridging ligands. A Mulliken analysis provides a spin population value of 4.88 e^- for the central Mn^{II} cation, slightly larger than at the other Mn^{II} cations (4.85 e^-), probably due to a larger localization induced by longer Mn−O bond distances. The Mn^{III} cations show spin population values between 3.85 and 3.88 e^-, indicative of a high degree of localization as a consequence of the poor mixing between the ligand and Mn^{III} $3d_{z^2}$ orbitals, expected for the long Mn−N bond distance induced by the Jahn−Teller effect.

Conclusions

The exchange coupling constants calculated using methods based on density functional theory provide an accurate description of the available experimental magnetic properties of the Mn_{10} and Mn_{19} complexes. All the exchange coupling interactions in such systems are ferromagnetic, giving the $S = 22$ and $S = 83/2$ ground states experimentally found. Magnetic susceptibility curves obtained from the calculated J values using quantum Monte Carlo simulations and, in the case of Mn_{10},

Table 4. Calculated Exchange Coupling Constants J (cm^{-1}) for Five Manganese Dinuclear Complexes,[40–44] $[Mn^{IV}_2(\mu\text{-O})_2(N\text{-Eth-sal})_2]$ (**1**), $[Mn^{III}_2(\mu\text{-O})(\mu\text{-OAc})_2(tacn)_2]^{2+}$ (**2**), $[Mn^{II}_2(OAc)_2(BpmpH)]^{+}$ (**3**), $[Mn^{II}_2(\mu\text{-O})_2(bispicMe_2en)_2]^{2+}$ (**4**), and $[Mn^{II}_2(\mu\text{-O})(\mu\text{-OAc})_2(TP\text{-}TACN)_2]^{2+}$(**5**)[a]

basis set			complexes				
Mn	other elements	functional	**1**	**2**	**3**	**4**	**5**
			Numerical				
TZP	DZ pseudo1	PBE	−376.3	+2.2	−25.1	−314.4	−11.9
DZP	DZ pseudo2	PBE	−347.3	+14.6	−20.8	−241.2	+5.7
			Gaussian				
ae TZP	*ae* DZ	PBE	−409.0	−20.7	−26.5	−311.0	−33.5
ae TZP	*ae* DZ	B3LYP	−190.6	+16.6	−13.4	−183.9	+8.9
			Experimental				
			−300	+18	−9.6	−201	+9.2

[a] The Siesta code was used with PBE functional and basis sets of different quality and two different pseudopotentials. The Gaussian calculations were carried out with the PBE and B3LYP functionals using the double-ζ basis set (DZ) of Schaefer et al.[33] for the main group elements and the triple-ζ one from the same authors for the manganese atoms (TZP).

combined with the exact diagonalization of the smallest blocks reproduce well the experimental curve. There are two types of exchange pathways, the first one with stronger ferromagnetic interactions through oxo and azido bridging ligands, and the second one through oxo and alkoxo bridging ligands. The role of the azido ligand seems to be less important than previously thought, probably due to the long Mn^{III}−N distances produced by a Jahn−Teller effect, since the calculated J values for Mn_{10} complexes with azides replaced by other linear ligands, such as hydroxo or thiocyanate, are also ferromagnetic and of similar strength. The weak ferromagnetic coupling found through the oxo−alkoxo exchange pathway can be explained by the nature of the Mn^{II}−Mn^{III} interactions and the high coordination numbers of the Mn^{II} cations (seven or eight) that results in long Mn−O bond distances to the bridging ligand.

The synergy between experimental and theoretical studies in the field of molecular magnetism has been shown to complement the synthesis of new unprecedented high-spin complexes with a detailed theoretical characterization of the magnetic interactions at the microscopic level.

Computational Details

In our calculations, we employed the experimental structures that take into account small structural effects induced by intermolecular interactions that may result in significant changes in the calculated exchange coupling constants, due to the strong dependence of the magnetic properties on structural parameters. Calculations with the B3LYP functional[28] were performed with the Gaussian03[29] and NWChem codes[30,31] using the quadratic convergence approach and a guess function generated with the Jaguar 6.5 code.[32] The triple-ζ all-electron Gaussian basis set proposed by Schaefer et al. was employed.[33] The results are summarized in Table 4.

Table 5. Calculated Exchange Coupling Constants J (cm^{-1}) and Metal Spin Populations for the Mn_{10} Complex $[Mn^{II}_4Mn^{III}_6O_4(N_3)_4(hmp)_{12}]^{2+}$ Using Gaussian and Numerical Basis Sets

	Gaussian B3LYP	Gaussian PBE	Siesta pseudo1 PBE	Siesta pseudo2 PBE
J_a	15.9	18.5	13.0	23.2
J_b	1.6	−1.8	−0.7	3.7
ρ (Mn^{II})	4.88	4.87	4.80	4.67
ρ (Mn^{III})	3.94	3.84	3.85	3.84

For the calculations performed with the Siesta program (Spanish Initiative for Electronic Simulations with Thousands of Atoms),[34–37] the GGA exchange-correlation functional proposed by Perdew, Burke, and Erzernhof (PBE) was used.[12] We took values of 50 meV for the energy shift and 200 Ry for the mesh cutoff that provide a good compromise between accuracy and computer time needed to calculate the exchange coupling constants.[13] Only valence electrons are included in the calculations, the cores being replaced by norm-conserving scalar relativistic pseudopotentials factorized in the Kleinman−Bylander form.[38] These pseudopotentials are generated following the procedure proposed by Trouiller and Martins[39] from the ground-state atomic configurations for all the atoms except for Mn, for which the Mn^{II} configuration $[Ne]3s^23p^64s^03d^5$ was employed. The core radii for the s, p, and d components of the Mn atoms are 1.4, 1.9, and 1.5 au, respectively, and we have included partial-core corrections for a better description of the core regions. The cutoff radii were 1.15 au for oxygen, nitrogen, and hydrogen atoms, 1.25 au for carbon, and 1.6 au for chlorine atoms.

This new pseudopotential (called hereafter pseudo2) employed for Mn atoms, describing the 3s and 3p orbitals with a numerical basis set, considerably improves the results compared to those obtained with a large core pseudopotential used previously (pseudo1).[14] The new results agree even better in some cases with the experimental data than those obtained with a Gaussian basis set and the hybrid B3LYP functional for a set of manganese dinuclear complexes (Table 4). The use of this functional also provides a correct description of the signs of the calculated J values for the Mn_{10} complex. The GGA functional (PBE) employed with Gaussian basis sets provides results somewhat different from those obtained with hybrid functionals, overestimating the antiferromagnetic contributions and giving a too-large spin delocalization on the ligands.[45] For instance, the J_b value calculated for the Mn_{10} complex with the PBE functional and Gaussian basis set (Table 5) has a wrong negative sign for this interaction, as happens also for the two ferromagnetic dinuclear complexes (Table 4). However,

(28) Becke, A. D. *J. Chem. Phys.* **1993**, *98*, 5648–5652.
(29) Frisch, M. J. *Gaussian 03* (Revision C.1); Gaussian, Inc: Pittsburgh, PA, 2003.
(30) Aprà, E. *NWChem 4.7*; Pacific Northwest National Laboratory: Richland, WA, 2005.
(31) Kendall, R. A.; Apra, E.; Bernholdt, D. E.; Bylaska, E. J.; Dupuis, M.; Fann, G. I.; Harrison, R. J.; Ju, J. L.; Nichols, J. A.; Nieplocha, J.; Straatsma, T. P.; Windus, T. L.; Wong, A. T. *Comput. Phys. Commun.* **2000**, *128*, 260.
(32) *Jaguar 6.0*; Schrödinger, Inc.: Portland, 2005.
(33) Schaefer, A.; Huber, C.; Ahlrichs, R. *J. Chem. Phys.* **1994**, *100*, 5829–5835.
(34) Artacho, E.; Gale, J. D.; García, A.; Junquera, J.; Martin, R. M.; Ordejón, P.; Sánchez-Portal, D.; Soler, J. M. *Siesta*, v.1.1; 2001 (http://www.uam.es/siesta).
(35) Soler, J. M.; Artacho, E.; Gale, J. D.; García, A.; Junquera, J.; Ordejón, P.; Sánchez-Portal, D. *J. Phys.: Condens. Matter* **2002**, *14*, 2745–2779.
(36) Artacho, E.; Sánchez-Portal, D.; Ordejón, P.; García, A.; Soler, J. M. *Phys. Stat. Sol. A* **1999**, *215*, 809–817.
(37) Sánchez-Portal, D.; Ordejón, P.; Artacho, E.; Soler, J. M. *Int. J. Quantum Chem.* **1997**, *65*, 453–461.
(38) Kleinman, L.; Bylander, D. M. *Phys. Rev. Lett.* **1982**, *48*, 1425–1428.
(39) Trouiller, N.; Martins, J. L. *Phys. Rev. B* **1991**, *43*, 1993–2006.
(40) Blanchard, S.; Blondin, G.; Riviere, E.; Nierlich, M.; Girerd, J.-J. *Inorg. Chem.* **2003**, *42*, 4568–4578.
(41) Glerup, J.; Goodson, P. A.; Hazell, A.; Hazell, R.; Hodgson, D. J.; McKenzie, C. J.; Michelsen, K.; Rychlewska, U.; Toftlund, H. *Inorg. Chem.* **1994**, *33*, 4105–4111.
(42) Torayama, H.; Asada, H.; Fujiwara, M.; Matsushita, T. *Polyhedron* **1998**, *17*, 3859–3874.
(43) Wieghardt, K.; Bossek, U.; Ventur, D.; Weiss, J. *Chem. Commun.* **1985**, 347–349.
(44) Bolm, C.; Meyer, N.; Raabe, G.; Weyhermuller, T.; Bothe, E. *Chem. Commun.* **2000**, 2435–2436.
(45) Ruiz, E.; Alvarez, S.; Cano, J.; Polo, V. *J. Chem. Phys.* **2005**, *123*, 164110.

in the calculations with PBE functional using numerical basis sets, the results are relatively similar to those obtained with the hybrid functional and Gaussian basis sets, giving in both cases a nice agreement with the experimental data.[13,14] The difference obtained using the same PBE functional between the Gaussian and numerical codes was noticed previously,[14] and the reason of such a difference could be related to the confinement of the wave function in the numerical code, resulting in a smaller delocalization of the spin density. For instance, in the case of complex **2** (Table 4), the Mulliken spin population for the Mn^{III} cations with PBE and Siesta is 3.918 e^- while the B3LYP and PBE values with Gaussian are 3.920 and 3.870 e^-, respectively. The comparison of these spin population values shows that the spin delocalization is very similar between the Siesta PBE values and those obtained with the B3LYP functional and Gaussian basis set, and consequently the J values are relatively similar.

Four calculations were performed on the $[Mn^{II}_4Mn^{III}_6O_4(N_3)_4(hmp)_{12}]^{2+}$ complex in order to obtain the two exchange coupling constants by least-squares fitting for the following spin configurations: a high-spin solution ($S = 22$), an $S = 2$ configuration with negative spin at all the Mn^{II} cations {Mn1, Mn2, Mn3, Mn4} (Figure 2), another one with negative spin at the Mn^{III} cations and $S = 6$ at {Mn6, Mn7, Mn8, Mn10}, and an $S = 14$ configuration with negative spin at {Mn7, Mn8}. For the Mn_{19} complex, nine spin distributions were calculated: the high-spin distribution ($S = 83/2$), an $S = 51/2$ configuration with negative spins at the atoms {Mn4, Mn5, Mn13, Mn14}, and eight distributions with the following total spin and metal atoms with negative spins: $S = 57/2$ {Mn5, Mn14}, $S = 47/2$ {Mn4, Mn10, Mn14, Mn19}, $S = 35/2$ {Mn2, Mn3, Mn4, Mn11, Mn12, Mn13}{Mn5, Mn6, Mn7, Mn14, Mn15, Mn16}, $S = 31/2$ {Mn2, Mn7, Mn8, Mn11, Mn16}, $S = 25/2$ {Mn1, Mn2, Mn3, Mn4, Mn11, Mn12, Mn13}, and $S = 13/2$ {Mn1, Mn8, Mn9, Mn10, Mn17, Mn18, Mn19}.

Acknowledgment. The research reported here was supported by the Dirección General de Investigación del Ministerio de Educación y Ciencia and Comissió Interdepartamental de Ciència i Tecnologia (CIRIT) through grants CTQ2005-08123-C02-02/BQU and 2005SGR-00036, respectively. The authors thankfully acknowledge the computer resources, technical expertise, and assistance provided by the Barcelona Supercomputing Center (Centro Nacional de Supercomputación). R.C. thanks the Ministerio de Educación y Ciencia for a Mobility Program grant to cover his stay in Barcelona.

Supporting Information Available: Complete refs 29 and 30; Cartesian coordinates and calculated energies for the high-spin state using the B3LYP functional and the Gaussian basis set of the Mn_{10} and Mn_{19} complexes. This information is available free of charge via the Internet at http://pubs.acs.org.

JA800092S